Original Paper

Experimental Study and Numerical Simulation of Cavity Oscillation in a Conical Diffuser

Changkun Chen[1], Christophe Nicolet[2], Koichi Yonezawa[1], Mohamed Farhat[2], Francois Avellan[2], Kazuyoshi Miyagawa[3], Yoshinobu Tsujimoto[2]

[1]Graduate School of Engineering Science, Osaka University
Machikaneyama 1-3, Toyonaka, 560-8531, Japan
[2]Laboratory for Hydraulic Machines, EPFL - Swiss Federal Institute of Technology
33 bis av. de Cour, Lausanne, CH-1007, Switerland
[3]Nagasaki R&D Center, Mitsubishi Heavy Industries, LTD
Fukahori-machi 5-717-1, Nagasaki, 851-0392, Japan

Abstract

Based on the one-dimensional stability analysis, the self-excited oscillation in hydraulic power generating systems was studied by a simple experiment and numerical simulation. It was shown that a cavity in a conical diffuser can cause surge. With the diffuser, a high amplitude and low frequency oscillation occurs at low cavitation number. This oscillation was not observed with the straight pipe. It was confirmed that the diffuser effect of the draft tube can be the cause of the full load surge in hydraulic power system. Numerical results were also analyzed to check the validity of the one-dimensional stability analysis.

Keywords: Draft tube surge, diffuser effect, cavitation.

1. Introduction

Securing stable operation is one of the most important issues in hydraulic power generating systems. In Francis turbines, draft tube surge is the most commonly identified phenomenon among pressure fluctuations. At low flow rate, the precessing motion of the vortex rope in the draft tube is the main cause of pressure fluctuation [1]-[3]. It has been found that a surge can occur even at full load. The behavior of full load surge in model test is reported by Prenat and Jacob [4] in 1986. Arzola et al. [5] found that in a real plant, modifying the shape of the runner cone can change the frequency of full load surge and the surge is well eliminated by air injection from the runner cone. Koutnik et al. [6] simulated the full load surge by representing the effect of the cavitation in the draft tube by cavitation compliance $C = -\partial V_C / \partial p_D$ and mass flow gain factor $\chi = -\partial V_C / \partial Q_D$, where V_C is the volume of the cavity, p_D and Q_D are pressure and flow rate downstream of the cavity. It was shown that the instability occurs when the absolute value of negative mass flow gain factor is larger than a certain value which depends on the value of cavitation compliance. This model was combined with the numerical analysis software SIMSEN to analyze the full load surge observed in a real plant [7]. Although Ref.[6] and [7] show that full load surge can be successfully simulated by using an appropriate value of mass flow gain factor, the flow mechanism determining the mass flow gain factor is not clear yet.

The previous study [8] established a one-dimensional analytical model to clarify the possibility of self-excited oscillation mechanism of the full load draft tube surge. Two sources of draft tube instability have been found. The first is the instability caused by the diffuser effect of draft tube. This destabilizing effect appears for all flow rate and the destabilizing effect increases as the increase of the flow rate. The second source of instability is caused by the swirl downstream of the runner, which destabilizes the system in part load operation and stabilizes in over load operation.

The destabilizing effect of the diffuser can be explained as follows. We consider the case when a diffuser is placed downstream of a cavitating part. It is assumed that the pressure is kept constant at the diffuser exit. If the cavity volume is increased and the flow rate through the diffuser is increased, the pressure at the cavity will be decreased since the pressure recovery in the diffuser is increased. Then the cavity volume would increase further. This positive feedback is the cause of the instability due to the diffuser effect.

In the present study, the cavitation instability caused by the diffuser effects is confirmed experimentally with a simple facility

using a conical diffuser and a straight pipe. At low cavitation number range, a low-frequency fluctuation occurs with the diffuser but not with the straight pipe. Numerical computation also simulates this fluctuation and the results are analyzed to check the validity of the one-dimensional stability analysis.

2. One-dimensional Analysis [8]

As shown in Fig. 1, we consider a system composed of an inlet pipe of length L_i and area A_i, a turbine runner, and a draft tube with the inlet and exit areas A_C and A_e, respectively. A cavity volume of V_C is assumed downstream of the turbine and upstream of the draft tube. Then, the continuity equation between upstream and downstream flow rates Q_1 and Q_2 is:

$$Q_2 - Q_1 = dV_C / dt \tag{1}$$

By applying unsteady Bernoulli's equation to the draft tube, we obtain,

$$p_a - p_{exit} = \rho \frac{L_e}{A_e} \frac{dQ_2}{dt} + \rho \frac{\zeta_2 - D}{2 A_e^2} Q_2^2 \tag{2}$$

where $L_e = \int (A_e / A(s)) ds$ is the effective length of the draft tube, $D=(A_e/A_c)^2-1$ the diffusion factor, ζ_2 the loss coefficient of the draft tube. For simplicity, ζ_2 is assumed to be a constant value. Equation (2) ignores the flow compressibility in the draft tube.
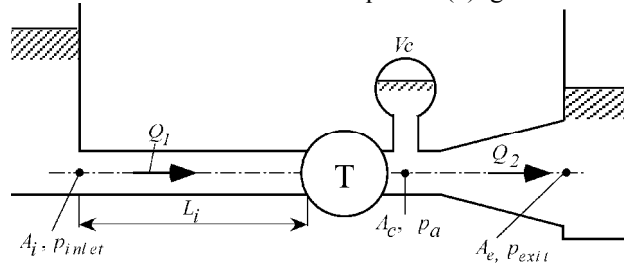

Fig. 1 Hydraulic system for the analysis

At off-design operating point, the discharge flow from the runner swirls and a vortex is formed. If the pressure p_C at the vortex center is lower than the vapor pressure, a cavity will appear. The volume of cavity can be considered to be a function of the core pressure p_C,

$$V_C = V_C(p_C) \tag{3}$$

The cavitation compliance C is defined by

$$C = -dV_C / dp_C \tag{4}$$

Due to the centrifugal force on the swirling flow, the core pressure p_c is lower than the ambient pressure p_a. Here, the effect of swirl is neglected and $p_C = p_a$ is assumed to examine only the diffuser effect.

Then, the continuity equation (1) can be expressed as

$$Q_2 - Q_1 = dV_C / dt = (dV_C / dp_C)(dp_C / dt) = -C(dp_C / dt) = -\rho C \frac{L_e}{A_e} \frac{d^2 Q_2}{dt^2} + \rho C \frac{D - \zeta_2}{A_e^2} Q_2 \frac{dQ_2}{dt} \tag{5}$$

The second term with dQ_2/dt represents the diffuser effect corresponding to the mass flow gain factor.

For stability analysis, it is assumed that $Q = \bar{Q} + \tilde{Q}(t) = \bar{Q} + \tilde{Q}_0 e^{j\omega t}$, where j is an imaginary unit. The steady component $\bar{Q}$ is much larger than the unsteady component $\tilde{Q}$. The complex frequency $\omega = \omega_R + j\omega_I$ shows the fluctuation frequency ω_R and the damping rate ω_I.

When assuming $\bar{Q}_1 = \bar{Q}_2 = \bar{Q}$, the unsteady part of Eq. (5) can be expressed:

$$\tilde{Q}_2 - \tilde{Q}_1 = -\rho C \frac{L_e}{A_e} \frac{d^2 \tilde{Q}_2}{dt^2} + \rho C \frac{D - \zeta_2}{A_e^2} \bar{Q}_2 \frac{d\tilde{Q}_2}{dt} \tag{6}$$

Equation (6) can be written as

$$\rho C \frac{L_e}{A_e} \frac{d^2 \tilde{Q}_2}{dt^2} + \rho C \frac{\zeta_2 - D}{A_e^2} \bar{Q}_2 \frac{d\tilde{Q}_2}{dt} + \tilde{Q}_2 = \tilde{Q}_1 \tag{7}$$

If we consider the case of $\tilde{Q}_1 = 0$, negative damping occurs when

$$D > \zeta_2 \tag{8}$$

This is caused by the diffuser effect of the draft tube. From Eq. (7) the frequency is given by

$$\omega_e = \sqrt{\frac{A_e}{\rho L_e C}} \tag{9}$$

This mechanism can be explained as follows. When Q_2 is increased, Eq.(2) shows that p_a will decrease if $D > \zeta_2$, due to the diffuser effect and Eq. (4) shows that the cavity volume V_C is increased since $C>0$. Then Eq.(1) shows that Q_2 will be increased further, if Q_1 is kept constant. This positive feedback is the cause of the instability due to the diffuser effect.
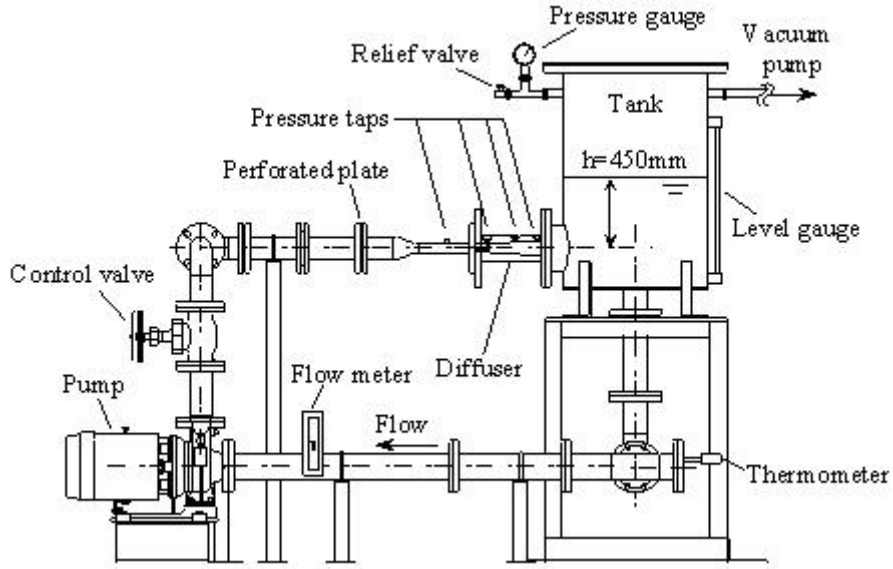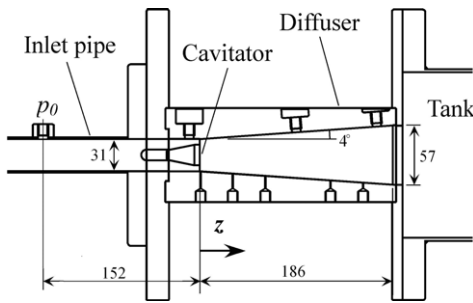
Fig. 2 Schematic of experimental facility.
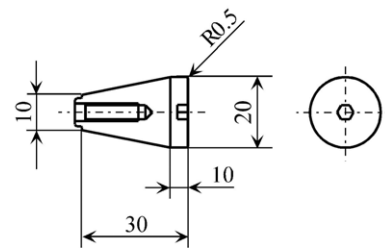

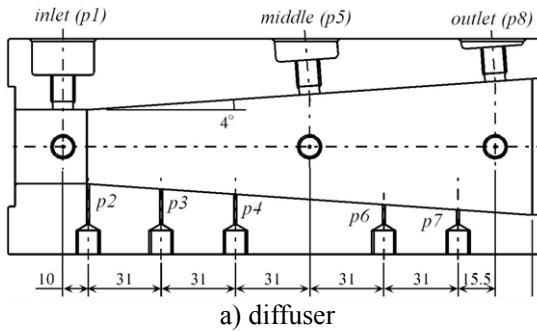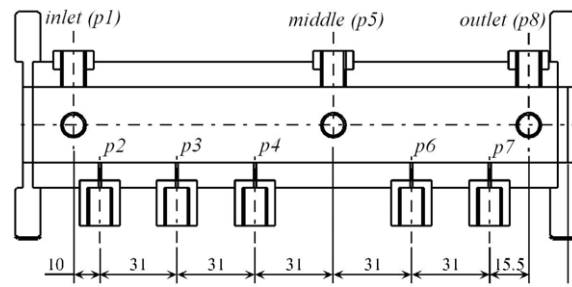**Fig. 3** Test section

Fig. 4 Cavitator shape.

a) diffuser

b) straight pipe

Fig. 5 Geometry and pressure taps displacement of diffuser and straight pipe

3. Experimental Study

3.1 Experimental facility and measurement

Figure 2 shows the framework of experimental facility. A cavitator is placed at the diffuser inlet to simulate the resistance of turbine runner and to trigger cavitation. The tank pressure downstream the diffuser is controlled by a vacuum pump to set the cavitation number. The working fluid is tap water at room temperature, degassed by the vacuum pump. The flow rate and fluid temperature are measured at the pump upstream.

Figure 3 shows the diffuser section. A conical diffuser and a straight pipe as shown in Fig.5 are used. The geometry of cavitator at the diffuser inlet is shown in Fig.4. Cavity occurs downstream the cavitator in the diffuser. Three dynamic pressure transducers p_1, p_5, p_8 are flush mounted along the diffuser and the straight pipe. Another pressure tap p_0 is placed at 152 mm upstream of the diffuser inlet. Additional five static pressure taps are used to measure the pressure distribution along the diffuser, as shown in Fig.5.

The dimensionless parameters mainly used in this study are:

Cavitation number $\sigma = (p_T - p_v)/(\rho u_i^2/2)$, pressure coefficient $\psi = (p - p_v)/(\rho u_i^2/2)$;

Reynolds number $Re = u_i d_i/\nu$, Strouhal number $St = fl/u_i$; Dimensionless cavity length $L = L_C/d_i$

where the reference velocity u_i is the average inlet velocity in the upstream pipe; the reference length d_i is the diffuser inlet diameter (31mm); p and p_v are the pressure on the diffuser wall and the vapor pressure. The tank pressure p_T is the pressure at the diffuser exit, evaluated from the pressure above the water level and the height of the water level. ν is the kinematic coefficient of viscosity and f is the pressure fluctuation frequency. L_C is the average cavity length measured from pictures recorded by high-

speed video. Note that the length *l* of the diffuser and the straight pipe has been used for the definition of Strouhal number.

3.2 Results and discussion

Figure 6 shows the variations of Strouhal number *St* of the pressure fluctuations with respect to cavitation number σ. Dimensionless cavity length *L* from visual observation is also shown.

At higher cavitation number range ($\sigma > 2$), a high-frequency fluctuation component *St* >1 occurs both with diffuser and straight pipe. This is called Type I oscillation and occurs when the cavity length is smaller than the diffuser inlet diameter. The frequency decreases as the value of σ decreases. The high-speed photography shows that the cavity length does not fluctuate obviously in Type I oscillation.

At lower cavitation number range ($\sigma = 0 \sim 2$), a low-frequency pressure fluctuation component occurs at *St*=0.2~0.4. This is called Type II oscillation. The frequency component is corresponding to the cavity length fluctuation frequency recorded by high-speed video. With the diffuser, Type II oscillation occurs when cavity length is larger than 1.5 times of diffuser inlet diameter (*L* >1.5), while it does not occur for the case of straight pipe. So it is considered that Type II oscillation is caused by the diffuser effect. With the straight pipe, the cavity length increases rapidly near σ=1.3 after keeping nearly the same value of *L*<1.0 while decreasing the value of σ.
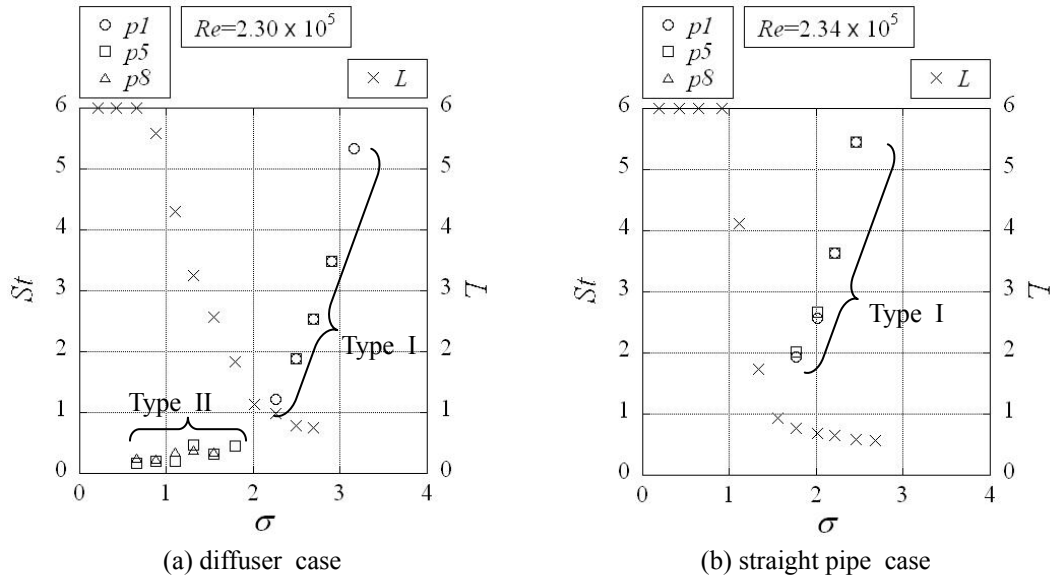

(a) diffuser case   (b) straight pipe case

Fig. 6 Strouhal number versus cavitation number and cavitation length.

σ=2.26 σ=2.22

σ=1.55 σ=1.10

simulation result at σ=1.55   simulation result at σ=1.10

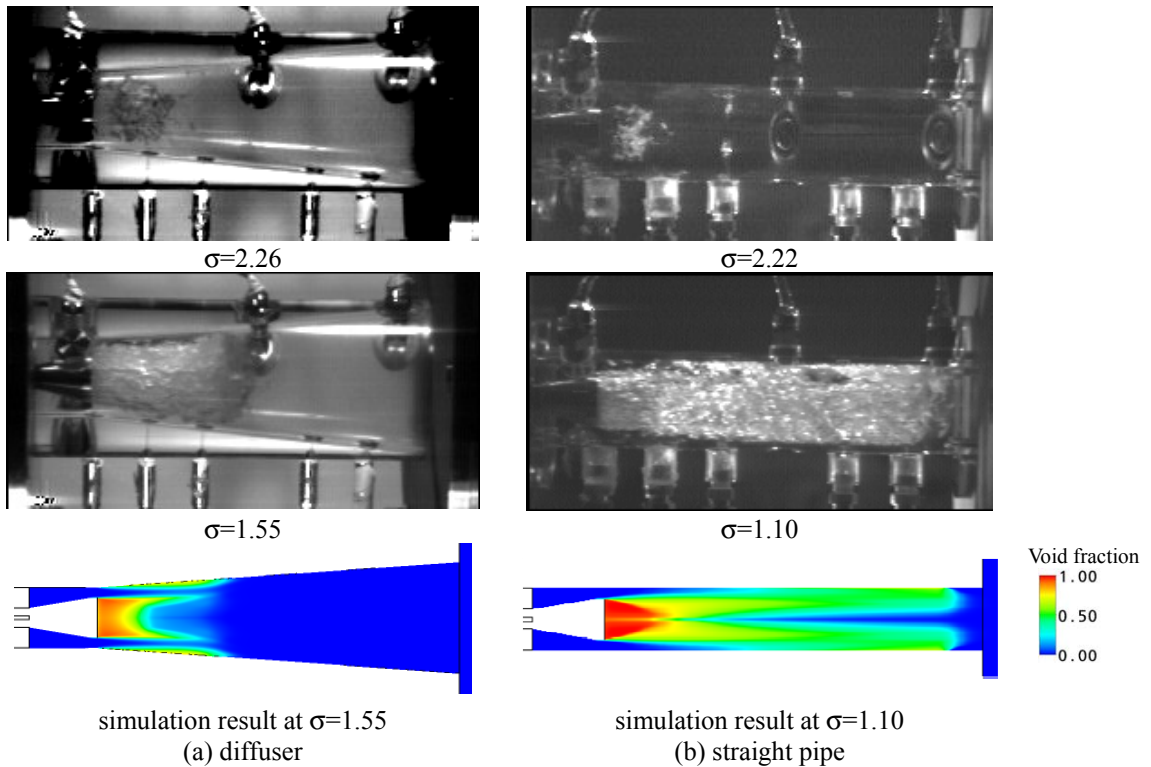(a) diffuser   (b) straight pipe

Fig. 7 Typical cavity pattern

Figure 7 shows the typical cavity pattern taken from high-speed video. First, we consider the case with the diffuser. At $\sigma = 2.26$ where Type I oscillation occurs, the cavity is detached from the downstream end of the cavitator. The cavitation is attached to the cavitator at $\sigma = 1.55$ where Type II oscillation occurs. With the straight pipe, the cavity appearance at higher cavitation number ($\sigma=2.22$) with Type I oscillation is nearly the same as with diffuser. However, the cavity develops rapidly ($\sigma=1.10$) and no Type II oscillation was observed. The experiment is carried out also for other Reynolds numbers ($Re=1.5 \sim 3.3\times10^5$). The characteristics of pressure fluctuation are not obviously affected by the Reynolds number.

Figure 8 shows the static pressure distribution on the diffuser wall. $z=0$ is the location of cavitator end at the diffuser inlet. The arrow shows the cavitation number range where Type II oscillation occurs. At higher σ value range, the pressure decreases to the minimum at $z=0$ and then increases rapidly downstream of the cavitator. This quick pressure recovery occurs at $z \le 2d$ for both diffuser and straight pipe cases. Thus, it is caused by the closure of the cavitator wake. Following this rapid increase, gradual pressure increase occurs for the diffuser. This is caused by the diffuser effect and it can not be found in the straight pipe. With smaller σ value, a region with nearly constant pressure appears. The length of the region is somewhat smaller than the cavity length shown in Fig.6. This is because the cavity trailing edge is lifted from the diffuser wall. A region of pressure recovery appears downstream of the constant pressure region. It is caused by the decrease of the cross-sectional area of the cavity wake and occurs for both cases of the diffuser and straight pipe. This pressure recovery also can cause instability, since the increase of downstream flow rate will cause the increase of the pressure recovery and results in the decrease of the pressure in the cavitating part. However, no Type II oscillation was found in the straight pipe.
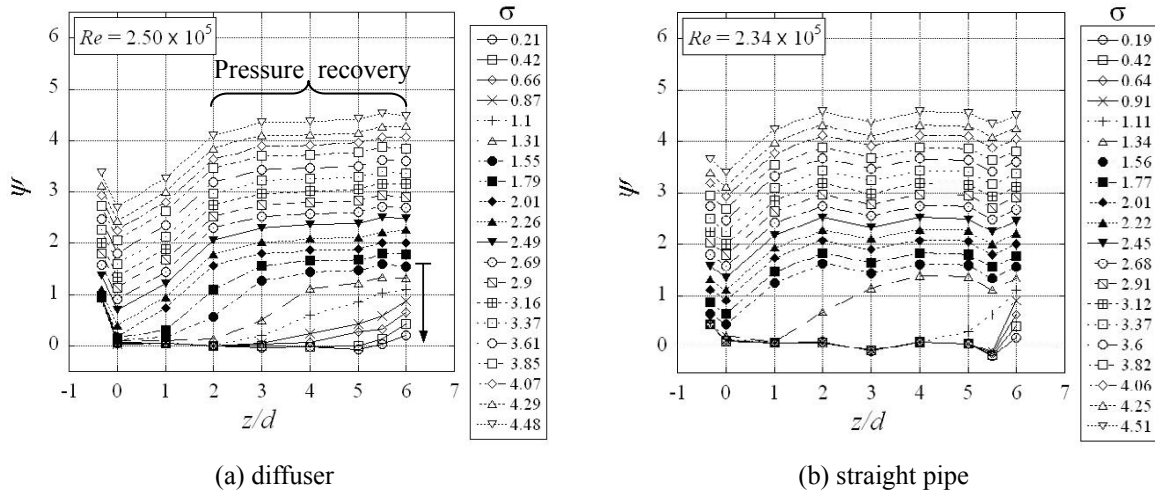

(a) diffuser   (b) straight pipe

Fig. 8 Static pressure distribution

4. Simulation

4.1 Computational scheme and grid

The numerical simulations are carried out with the commercial CFD software ANSYS CFX 11.0 package. For the spatial discretization, "High-Resolution Scheme" is applied in order to achieve 2nd order accuracy. For temporal discretization, the 2nd backward Euler scheme is applied. For turbulence treatment, the RANS k-ε model is used. The interface mass transfer for cavitation is modeled with a simplified Rayleigh Plesset equation. Homogeneous model is applied for multiphase flow treatment. The cavitating simulations are transient, starting from the non-cavitating results with a time step size of 0.0005 second, corresponding to about 200 steps within a period of Type II oscillation.

Figure 9 illustrates the computational domain for diffuser and straight pipe, both composed of approximately 800,000 structured hexahedral elements. The uniform axial flow of 300 L/min ($Re = 2.1\times10^5$) was given at the inlet boundary. Pressure was fixed constant at the outlet boundary. The wall boundary condition was imposed to be no slip and smooth wall.
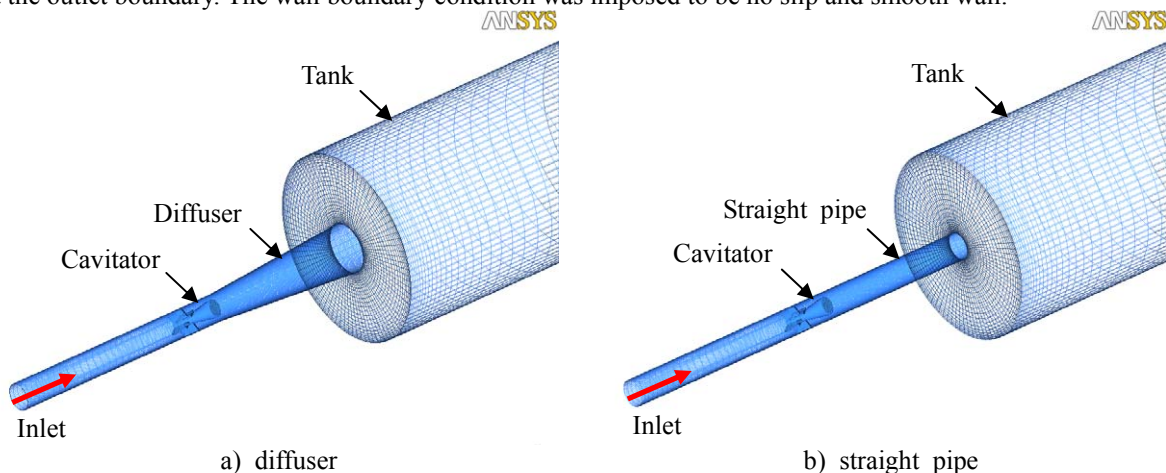

a) diffuser   b) straight pipe

Fig. 9 Computational Grids

4.2 Results

The typical cavity patterns under σ=1.55 are shown in Fig.7. It is shown that the simulated cavity length is comparable but slightly shorter than the experimental results. In Fig.10, the static pressure distribution is compared with the experiment result. It also shows the difference due to shorter cavity length. At high cavitation number range of σ>2, simulation shows no cavitation occurring in the diffuser or pipes. Thus, Type I oscillation could not be simulated.

Type II oscillation in the experiment can be simulated in a lower cavitation number range for the case with the diffuser. The time-series pressure data are shown in Fig.11 at σ =1.55 with the diffuser. The pressure at p_1, p_2 and p_3 is kept constant at vapor pressure because these points are within the cavitation zone. The time-series pressure data show nearly periodic oscillation at points $p_4 \sim p_8$. The amplitude decreases as we approach the diffuser exit. The predicted fluctuation frequency is $St = 0.14{\sim}0.19$, which is smaller than the measured value St=0.2~0.4. The Strouhal number is compared with the experimental value in Fig.12. With the straight pipe, this pressure fluctuation does not occur, which is the same as the experiment.
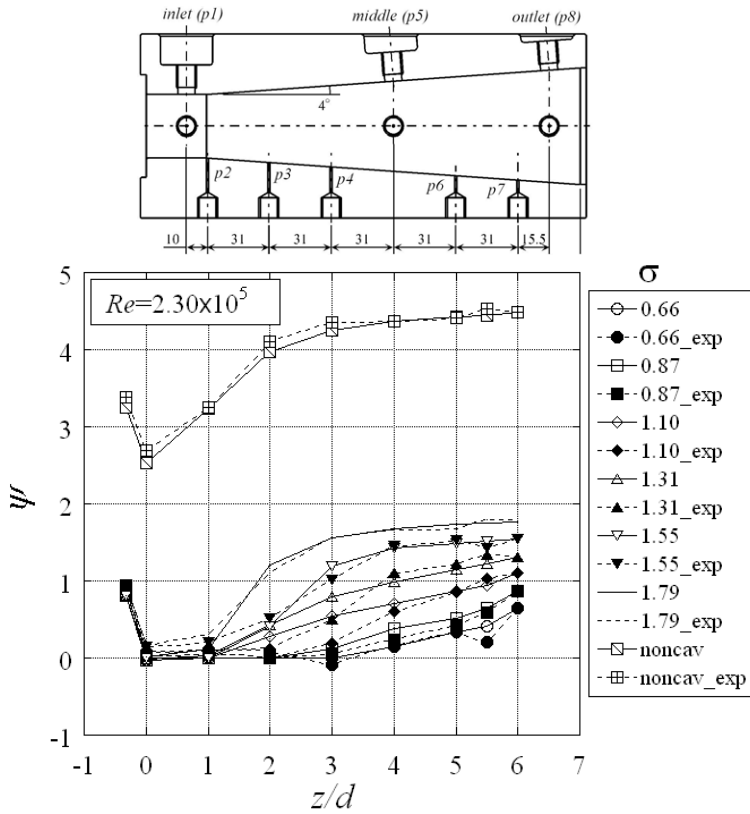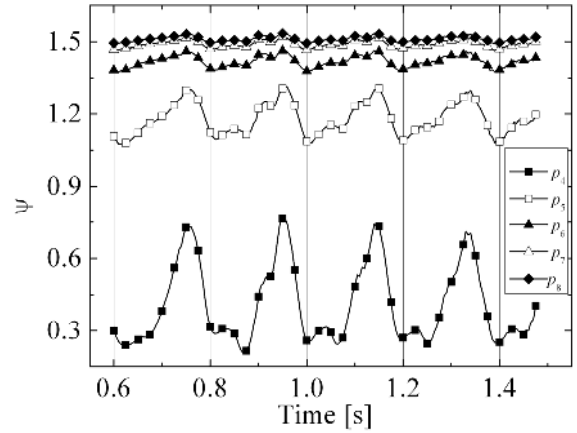

Fig. 11 Pressure fluctuation in the diffuser at σ=1.55

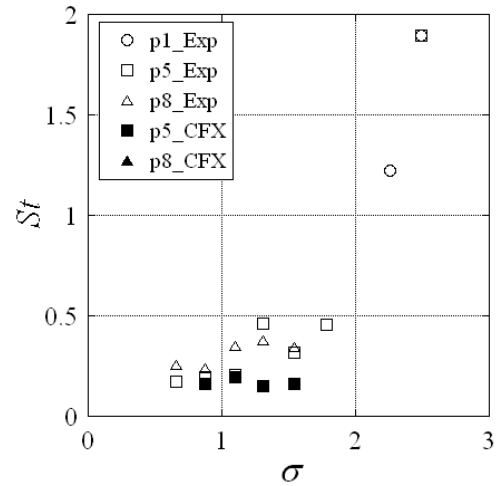**Fig. 10** Pressure distribution of diffuser case

Fig. 12 Strouhal number of fluctuations

4.3 Correlation with the one-dimensional model

In the one-dimensional model, the continuity equation (1) across the cavitating region and the unsteady Bernoulli equation (2) in the diffuser are combined to derive the characteristic equation (7) of the hydraulic system. Thus, in order to check the validity of the analytical model, the continuity and unsteady Bernoulli equation are examined using the simulation results.

4.3.1 Continuity equation

The simulation result of diffuser case at σ=1.55 is chosen to analyze the pressure fluctuation. In the one-dimensional model, Eq.(1) shows the continuity between cavity upstream and downstream flow rates. The difference of upstream flow rate Q_1 and downstream flow rate Q_2 and the time derivative of cavity volume V_C is plotted in Fig.13. Caused by the resistance at the cavitator and the larger mass in upstream penstock, Ref.[8] shows that the upstream flow rate Q_1 gives smaller fluctuation than downstream flow rate Q_2 and was kept to be constant in the simulation. This is also confirmed in the experiment, since no pressure fluctuation was observed at the inlet (p_1). The cavity volume V_C was evaluated by integrating the void fraction over entire computational domain: $V_C = \int f_C dV$. The result shows the flow rate difference Q_2 - Q_1 has the same tendency with the time derivative of V_C.

However, dV_C/dt evaluated from the void fraction is smaller than the flow rate difference. This suggests the incompleteness of the present simulation and higher spacial and temporal resolutions are needed. It should be mentioned that the agreement between Q_2 - Q_1 and dV_C/dt is sensitive to the time step length Δt. Better agreement is achieved when Δt is decreased from 0.0025 s to 0.0005 s. However, little further improvement can be obtained when Δt is decreased from 0.0005 s to 0.0001 s. Considering the computation time, the time step Δt =0.0005 s is used.
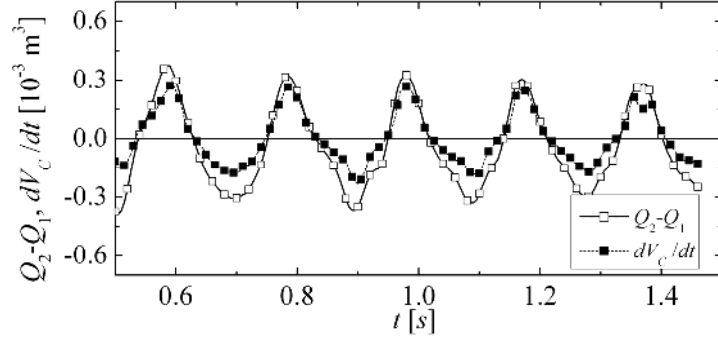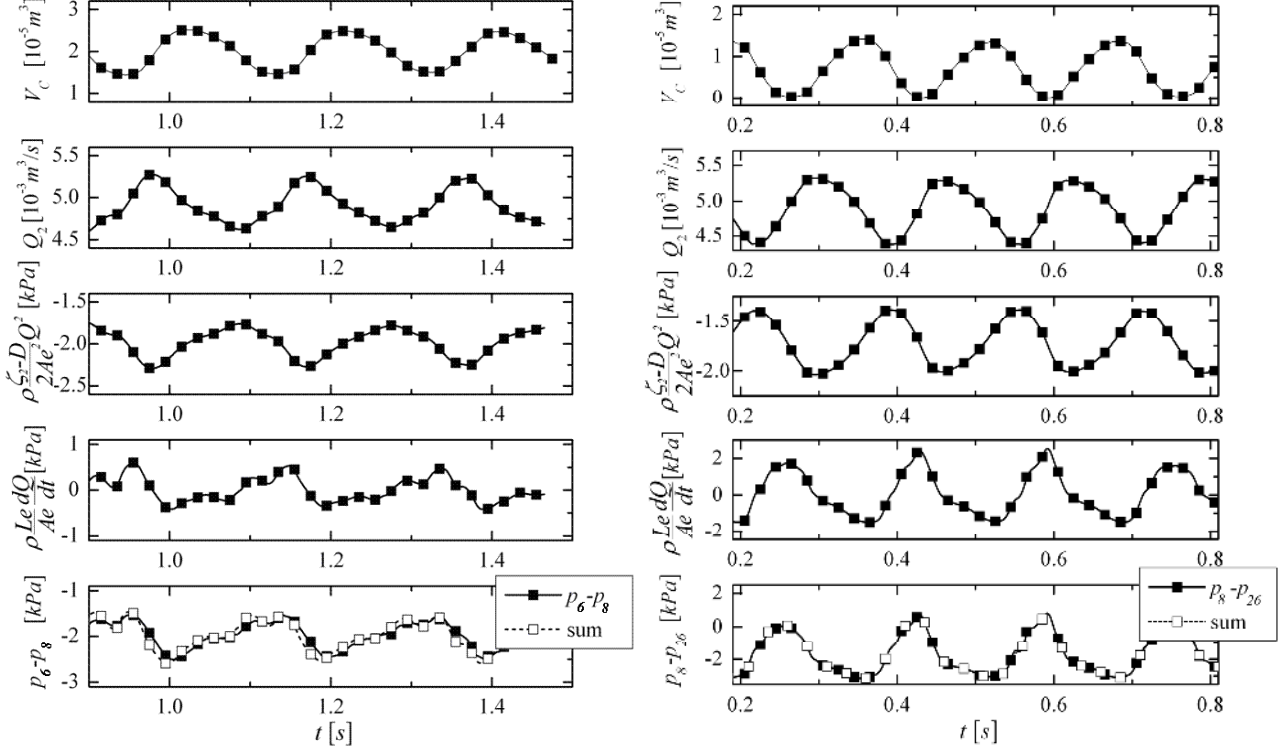
Fig. 13 Time-series flow rate difference and cavity volume change rate ($\varDelta t$ =0.0005 s)

(a) Diffuser (σ=1.55) (b) Extended diffuser (σ=1.82)

Fig. 14 Time-series data of the terms in unsteady Bernoulli equation (2)

4.3.2 Evaluation of loss coefficients, diffusion factor, and effective diffuser length

The characteristic equation (7) shows that the value of ζ_2 -D determines the stability and the value of effective length L_e determines the frequency of oscillation. Since these factors are traced back to the Bernoulli equation (2), the value of these factors are evaluated from the examination of the simulation results associated with Eq.(2). The pressure recovery between the pressure taps p_6 and p_8 is examined. This is to avoid the effect of cavity wake: the cavity trailing edge at σ=1.55 is well upstream of p_6.
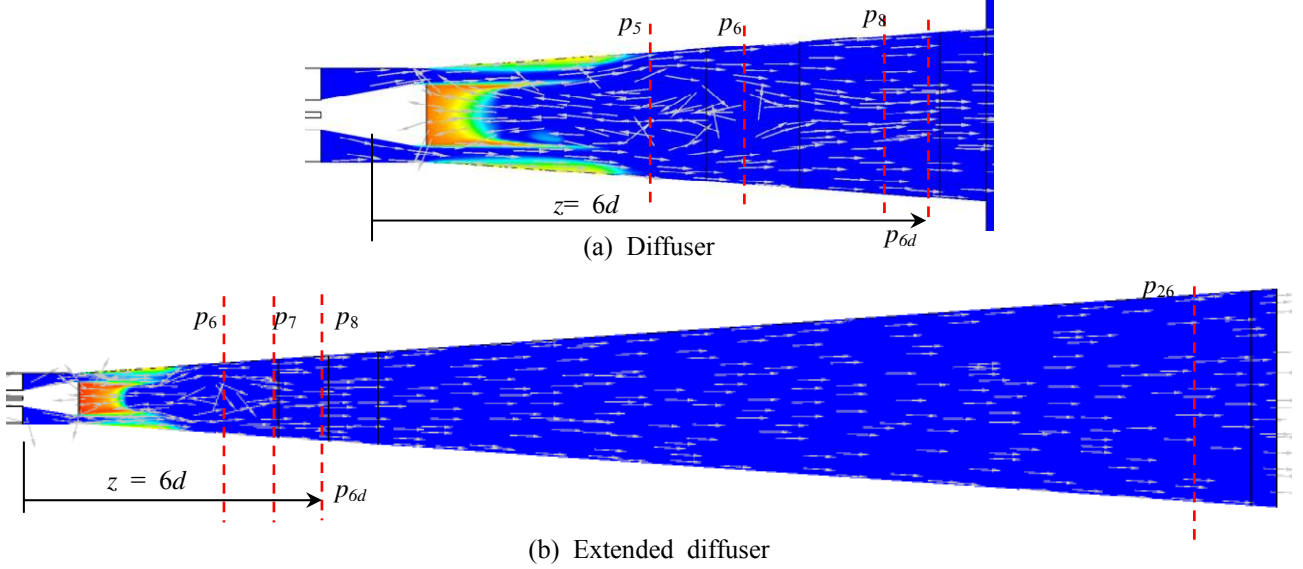
Figure 14 shows the plots of V_C, Q_2 and p_6-p_8 against time. p_6-p_8 is separated into the components of ρ (L_e/A_e) dQ_2/dt and ρ (ζ_2-D) $Q_2^2/ (2A_e^2)$ by using a least square curve fit assuming that ρ (L_e/A_e) and $\rho(\zeta_2$-D) /($2A_e^2$) are constants. In the bottom of Fig.14, the dashed curve with white points is the sum of the separated components compared with p_6-p_8 shown by the solid curve with black points. The agreement of these curves shows the expression of Bernoulli equation (2) is adequate. The values of ζ_2-D and L_e thus determined are shown in Table 1 as compared with the values evaluated from the geometry. The results of similar analysis for the straight pipe at σ=1.45 is also shown. For the straight pipe analysis, the pressure fluctuation with the half amplitude of $\Delta\psi$ = 0.0456 was applied at the pipe exit to realize oscillation. For the evaluation from the geometry, $\zeta_2=k(A_e/A_c-1)^2$ and $\zeta_2=kl/d_i$ are used for the diffuser and straight pipe, respectively, where k is the coefficient related to the diffusion angle, Reynolds number and pipe roughness[9]. Both the $|\zeta_2$-D| and L_e from simulation are much larger than the values evaluated from the geometry. This is considered to be caused by the effect of cavity wake which is close to p_6, as shown in Fig.15 (a). In order to confirm this, the lengths of the diffuser and straight pipe are extended to l=24d and the analysis was carried out for the region between z=6d (p_8) and 23.5d (p_{26}) from the inlet, as shown in Fig.15 (b). The simulation result of extended diffuser at σ=1.82 is chosen to analyze. The results are also shown in Table 1. Better agreement between the results from simulation and from geometry for ζ_2-D was achieved.

The time-average pressure distribution can be related to the coefficient ζ_2-D by Eq.(2). The values from the averaged steady pressure distribution are also shown in Table 1. The values from unsteady and steady pressure are nearly the same. The agreement between the values from geometry and simulation is worse for L_e/d, except for the case of extended straight pipe.

In any case, the value of ζ_2-D is negative for the diffuser and positive for straight pipe. The negative value of ζ_2-D is the cause of the instability of the diffuser.

Table 1 Evaluation of ζ_2-D and L_e

		ζ_2-D			L_e /d	
		Simulation	Geometry	Averaged pressure distribution	Simulation	Geometry
Diffuser	(σ=1.55)	-0.918	-0.656	-0.929	2.701	1.702
Extended Diffuser	(σ=1.82)	-27.714	-26.138	-26.405	41.421	19.894
Pipe	(σ=1.45)	0.487	0.006	0.485	8.729	1.500
Extended Pipe	(σ=1.14)	0.311	0.271	0.312	17.402	17.500

(a) Diffuser

(b) Extended diffuser

Fig. 15 Displacement of monitoring planes at extended diffuser

4.3.3 Cavitation compliance and displacement work transfer

Figure 16 (a) shows the plot of $\rho\,(L_e/A_e)\,dQ_2/dt$, $\rho(\zeta_2$-$D)Q_2^2/\,(2A_e^2)$ and $p_6 - p_8$ against cavity volume V_C under cavity oscillation at σ=1.55. The plot of loss term $\rho(\zeta_2$-$D)Q_2^2/\,(2A_e^2)$ shows a Lissajous curve in counter clockwise direction. This means that the cavity volume fluctuation delays behind flow rate fluctuation and the displacement work $\int \rho \dfrac{\zeta_2 - D}{2A_e^2} Q_2^2 dV_C$ is negative. Since it

is assumed that the upstream flow rate is kept constant, the negative cavity displacement work means that the downstream flow fluctuation provides positive displacement work to the cavity. This shows the important effect of diffuser to provide energy to the oscillation, as discussed also in Ref.[8]. The plot of inertia term $\rho\,(L_e/A_e)\,dQ_2/dt$ shows that the displacement work

$\int \rho \dfrac{L_e}{A_e} \dfrac{dQ_2}{dt} dV_C$ is close to 0. By using $dV_C/dt=Q_2$, $\int_0^T \dfrac{dQ_2}{dt} dV_C = \int_0^T Q_2 \dfrac{dQ_2}{dt} dt = \int_0^T \dfrac{1}{2}\dfrac{d}{dt}\left(Q_2^2\right) dt = 0$, where T is the period

of oscillation. This shows that the displacement work done by the inertia pressure should be zero. Thus, the total displacement work should be negative, which shows a counter clockwise Lissajous curve as expected in the bottom of Fig.16(a). The results with extended diffuser is similar, as shown in Fig.16(b). We should note that the mean slope of the plot is caused by the inertia effects.

The cavitation compliance C is defined by Eq.(4). Three methods were examined to evaluate the value of C from the results of simulation. The first is the quasi-steady evaluation from the averaged cavity volume at different cavitation numbers. In the linear model in section 2, it is assumed that the cavity volume V_C is a function of the pressure p_C near the cavity. In practical case, the pressure on the cavity is kept nearly constant at vapor pressure. So we need to determine the appropriate location where p_C is defined. However, the pressure at an arbitrary position downstream of the cavity changes linearly with the tank pressure. And the cavitation compliance is defined as the change of cavity volume due to the change of ambient pressure. We can determine the value of cavitation compliance using the pressure at an arbitrary downstream position. For this reason we use the pressure p_{6d} at z=6d. Figure 17 shows the plot of V_C against $\sigma_{6d} = (p_{6d} - p_v)/(\rho\,u_i^2\,/2)$ for original and extended diffusers. Since p_{6d} is slightly lower than the pressure at the tank exit, σ=1.55 corresponds to σ_{6d} =1.53 for the original diffuser. Based on this plot, the quasi-steady cavitation compliance can be evaluated from C=-$\partial V_{ave}\,/\,\partial p_{6d}$.

The second method is from the mean slope of the plot of cavity volume fluctuation as shown in Fig.16. Since the amplitude of pressure fluctuation depends on the location of the pressure measurement, the value of C thus determined depends on the location where the pressure fluctuation is measured. The downstream flow rate changes in the unsteady evaluation while it is kept constant in quasi-steady evaluation.
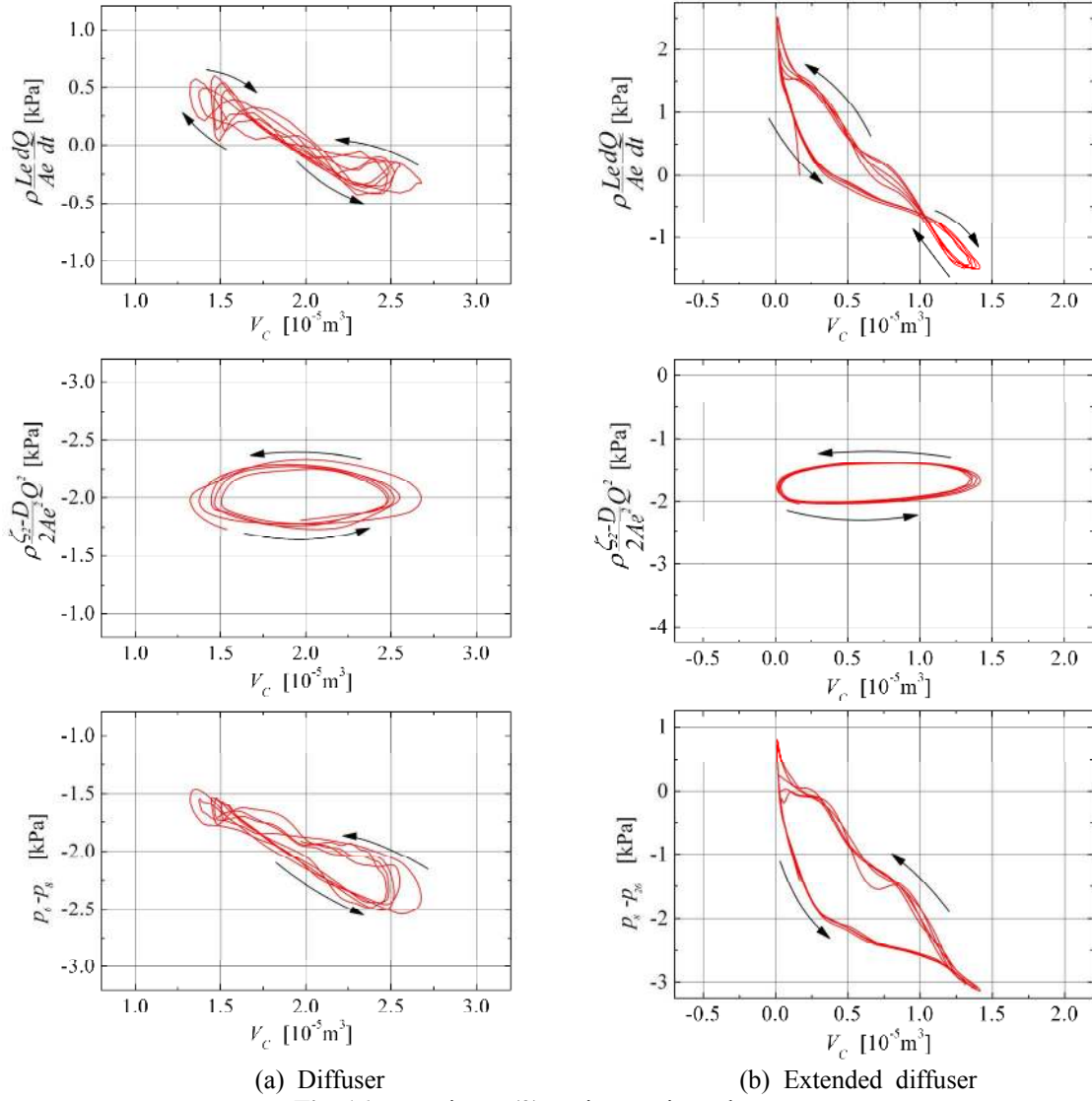
(a) Diffuser   (b) Extended diffuser

Fig. 16 Terms in Eq.(2) against cavity volume V_C.

The third method is the evaluation from Eq. (9) or $C = A_e /(\rho L_e \omega_e^2)$. This value also depends on the location where and how the value of L_e is evaluated. Here we use the values of L_e evaluated from the unsteady simulation at various axial locations as summarized in Table 1.

Table 2 compares the values of C evaluated from the above three methods. The values of C agree between quasi-steady and unsteady evaluation if we use the pressure fluctuation at an appropriate axial location. The values from frequency are significantly larger than the quasi-steady and unsteady values. This suggests that the values of L_e used are significantly smaller. The comparison with the values from unsteady evaluation shows that, the axial location for the evaluation of L_e should be more upstream than the location of pressure fluctuation for the evaluation of cavitation compliance. This suggests the importance of the inertia of the fluids around the cavity wake.
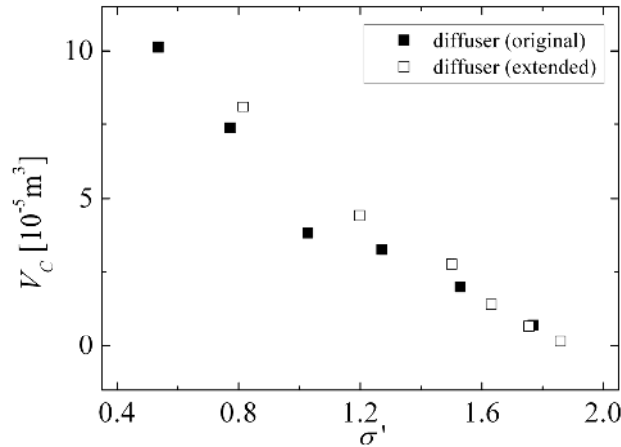

Fig. 17 Averaged cavity volume at various cavitation numbers

Table 2 Cavity compliance C from V_C of diffuser case

10^{-9} [m^3/Pa]	From quasi-steady cavity volume $C=-\partial V_{ave}$ / ∂p_{6d}	From unsteady cavity volume $C=-\partial V$ / ∂p_a	From frequency $C= A_e$ /($\rho L_e \omega_e^2$)
Diffuser (Original) at σ'=1.53 (σ=1.55)	3.34	7.02 ($p_a = p_6$) 2.58 ($p_a = p_5$)	30.01 (L_e at p_6) 6.54 (L_e at p_5)
Diffuser (Extended) at σ'=1.50	3.45	5.27 ($p_a = p_8$) 4.01 ($p_a = p_7$) 2.40 ($p_a = p_6$)	24.35 (L_e at p_8) 20.16 (L_e at p_7) 12.37 (L_e at p_6)

5. Conclusion

It was shown by a simple experiment and numerical simulation that a cavity in a diffuser can cause surge. In the experiment, a higher frequency oscillation is observed at higher cavitation number both in the diffuser and straight pipe. The frequency decreases as the cavitation number decreases. This type of oscillation could not be simulated by the CFD. With the diffuser, a high amplitude and low frequency oscillation occurs at low cavitation number where the cavity length is larger than 1.5 times of the diffuser inlet diameter. This oscillation was not observed with the straight pipe. This type of oscillation could be simulated by CFD, for the case of diffuser but no oscillation occurs with the straight pipe. Thus, it was confirmed experimentally and numerically that the diffuser effect of the draft tube can be the cause of the full load surge in hydraulic power stations.

The pressure recovery coefficient ζ_2- D of the diffuser and the effective diffuser length L_e were evaluated by separating the pressure fluctuation at the end of the cavity into the component proportional to the square of the flow rate and the component proportional to the time derivative of the diffuser flow rate. It was found that the value of ζ_2-D is negative for the diffuser and much larger than the value expected from the geometry of the diffuser. This value is positive for the straight pipe, supporting the result of one-dimensional stability analysis that, the pressure recovery in the diffuser causes the instability. The effective length of the diffuser L_e was also larger than the value from diffuser geometry. The value of cavitation compliance C was evaluated by three methods: quasi-steady evaluation from averaged cavity volume at different cavitation numbers, unsteady evaluation from cavity volume and pressure fluctuation, and the evaluation from the observed frequency. The unsteady evaluation agrees with quasi-steady value if we use pressure fluctuation at appropriate location. The value from the frequency is significantly larger if we use the effective length evaluated downstream of the cavity trailing edge. Perhaps we need to take account of the inertia effect of the fluid around the cavity wake when evaluating the cavitation compliance from frequency. The displacement work of the cavity was also discussed. The displacement work associated with the pressure recovery was negative, suggesting that the displacement work is transferred from the diffuser to the cavity.

Nomenclature

A_C	Inlet area of draft tube [m^2]	p_v	Vapor pressure [Pa]
A_e	Exit area of draft tube [m^2]	p_T	Tank pressure [Pa]
A_i	Area of inlet pipe [m^2]	Q_1	Flow rate upstream of cavity region [m^3/s]
C	Cavitation compliance [m^{3}s^2/kg]	Q_2	Flow rate downstream of cavity region [m^3/s]
D	Diffusion factor, =$(A_e /A_C)^2$-1	Re	Reynolds Number, = $u_i d_i /\nu$
d_i	Diffuser inlet diameter, 0.031 [m]	St	Strouhal number, = fl/u_i
f	Pressure fluctuation frequency [Hz]	t	Time [s]
f_C	Void fraction	u_i	Average inlet velocity [m/s]
j	Imaginary unit	V_C	Cavity volume [m^3]
L_C	Average cavity length [m]	χ	Mass flow gain factor [s]
L_e	Effective length of draft tube [m]	θ	Opening angle of diffuser, 14 [deg]
L_i	Length of inlet pipe [m]	ν	Kinematic coefficient of viscosity [m^2/s]
l	Diffuser length, 0.186 [m]	σ	Cavitation number, = $(p_T-p_v)/(0.5\,\rho u_i^2)$
p	Pressure [Pa]	ω	Complex frequency [rad/s]
p_a	Ambient pressure at cavity region [Pa]	ψ	Pressure coefficient, = $(p -p_v)/(0.5\,\rho u_i^2)$
p_C	Cavity core pressure [Pa]	ζ_2	Loss coefficient of the draft tube
p_{exit}	Pressure at exit of draft tube [Pa]		

Reference

[1] Nishi, M., "Surging Characteristics of Conical and Elbow Type Draft Tubes," Proceeding of the 12th IAHR Symposium on Hydraulic Machinery and System, Stirling, 1984, pp. 272-283.
[2] Nishi, M., Matsunaga, S., Kubota, T., Senoo, Y., "Flow Regimes in an Elbow-Type Draft Tube". Proceeding of the 11th IAHR Symposium on Hydraulic Machinery and System, Amsterdam, 1982, pp. 1-13, paper 38.

[3] Nishi, M., Wang, X., Okamoto, M., Matsunaga, S., "Further Investigation on the Pressure Fluctuations Caused by Cavitated Vortex Rope in an Elbow Draft Tube," In Cavitation and Gas Fluid Flow Machinery and Devices (1994), ASME, pp. 63-70.

[4] Prenat, J-E., Jacob, T., "Investigating the Behavior at High Load of a Francis Turbine Model," 13th IAHR Symposium, Montreal, 1986.

[5] Arzola, F., Azuaje, C., Zambrano, P., Gulbrandsen, G., "Undesired Power Oscillations at High Load in Large Francis Turbines. Experimental Study and Solution," 23rd IAHR Symposium, Yokohama, 2006.

[6] Koutnik, J., Pulpitel, L., "Modeling of the Francis Turbine Full-Load Surge," Modeling, Testing and Monitoring for Hydro Power Plants, Lausanne, 1996.

[7] Koutnik, J., Nicolet, C., A.Schoul, G., Avellen, F., "Overload Surge Event in a Pumped- Storage Power Plant," 23rd IAHR Symposium, Yokohama, 2006.

[8] Chen, C., Nicolet, C., Yonezawa, K., Farhat, M., Avellen, F., Tsujimoto, Y., "One-Dimensional Analysis of Full Load Draft Tube Surge," ASME Journal of Fluids Engineering, vol.130, Issue 4, 041106.

[9] Sabersky, R., 1999, "Fluid Flow: A First Course in Fluid Mechanics, 4th ed.," Prentice-Hall, New Jersey.